

# Exploring two Universal Extra Dimensions at the CERN LHC

Debajyoti Choudhury<sup>1</sup>, Anindya Datta<sup>2</sup>, Dilip Kumar Ghosh<sup>3</sup> and Kirtiman Ghosh<sup>4</sup>

<sup>1)</sup> *Department of Physics and Astrophysics, University of Delhi, Delhi 110 007, India*

<sup>2)</sup> *Department of Physics, University of Calcutta, 92 A.P.C. Road, Kolkata 700 009, India*

<sup>3)</sup> *Department of Theoretical Physics, Indian Association for the Cultivation of Science, 2A & 2B Raja S.C. Mullick Road, Kolkata 700 032, India*

<sup>4)</sup> *Harish-Chandra Research Institute, Chhatnag Road, Jhunsi, Allahabad 211 019, India*

## Abstract

We discuss the signatures, at the LHC, of the (1,0)-th Kaluza-Klein (KK) gluon and quarks in the framework of the two universal extra dimensional (2UED) model. Once produced, these particles typically suffer a cascade of decays terminating in the Dark Matter candidate apart from Standard Model particles. In this article, we are interested in focus on a particular signature of 2UED wherein the final state comprises of at least four jets in association with a hard photon and missing transverse energy. Several kinematic cuts are devised to enhance the signal to background ratio. Finally, as a road map to parameter determination at the LHC, we point out an interesting correlation between the peak position of the  $M_{eff}$  distributions with the compactification radius  $R$  and the cut-off scale  $M_s$ .

## 1 Introduction

Apart from finding out the so far elusive Higgs boson, the other main aim for the Large Hadron Collider (LHC) experiments is to explore any new dynamics operative at the TeV regime. As of now, the Standard Model (SM) remains very successful in explaining almost all of the experimental data related to elementary particle physics. Some discrepancies (mostly in flavour physics) do remain though, and while the statistical significance of each may not be a overriding cause of concern, together, they point to the tantalizing prospect of some new physics being just around the corner. Moreover, certain other inadequacies of the SM remain, e.g. the hierarchy problem, the lack of a Dark Matter candidate, an understanding

of neutrino masses, a lack of sufficient baryogenesis etc. Such issues have led to a plethora of new physics models being proposed. In this endeavour, models defined in more than three spatial dimensions need special attention.

Originally, extra dimensions had been proposed as a way to achieve unification of gravity and electrodynamics. Although, the initial constructions were beset with problems and soon rendered irrelevant, in later years, extra dimensions found a natural place in string theory. However, traditionally such extra dimensions were sought to be compactified with a radius too small to be of any phenomenological consequence. On the other hand, in recent years, (large) extra dimensions have been invoked to solve the hierarchy problem of the SM. In the models proposed by Arkani-Hamed, Dimopoulos and Dvali [1] and Randall and Sundrum [2], for example, the SM is confined to a sub-space of the  $1 + (3 + \delta)$  dimensional manifold, while gravity can propagate into all of the  $4 + \delta$  dimensions. On the contrary, in another class of models, some or all the SM fields can propagate into space beyond the usual  $1 + 3$  dimensions. While the name Universal Extra Dimensional (UED) model [3] strictly applies only to the case wherein each of the fields can percolate to all of the dimensions, the usage is often expanded to include scenarios wherein at least some of the SM fields propagate in more than four dimensions. Apart from a very rich phenomenology (which can be probed by the LHC), these models offer gauge coupling unification at a relatively low scale of energy [4–6], and naturally contain a weakly interacting massive stable particle, which can be a suitable candidate for cold dark matter [7–10]. While the simplest UED scenario would have only one extra dimension (*minimal UED* or mUED model), a particularly interesting variant is the eponymous *two Universal Extra Dimension (2UED)* model [11,12]. By definition, all the SM particles propagate in the entire  $1 + 3 + 2$ -dimensional space-time. Apart from providing a cold dark matter candidate [15], this model naturally suppresses proton decay rate to below the current constraints [13] as well as predicts the number of fermion generations [14], the last features rendering it superior to the minimal UED model. Although other variants of the 2UED model have been proposed since [19], we shall restrict ourselves to the simplest one.

For the sake of simplicity, let us assume that the two extra space-like dimensions have the same size. Furthermore, let us assume that the gauge structure as well as the particle content is the same<sup>1</sup> as in the SM. Consequently, after compactification (discussed in detail in

---

<sup>1</sup>Note that such a construction would be untenable in the mUED as parity is undefined in five dimensions.

a following section), the physical spectra will contain, apart from the SM particles, respective double towers of Kaluza-Klein (KK) excitations, with each excitation being specified by two integers,  $(i, j)$ , called the KK-numbers. In addition, the 5th and 6th components of the gauge bosons will appear in the low-energy theory as scalars transforming under the respective adjoint representations. Phenomenology of these spinless adjoints have been investigated in detail in Refs. [16–18, 20–22].

In this article, we will discuss, instead, search strategies for the strongly interacting  $(1, 0)$ -mode particles, as their production is favoured at the LHC. Once produced, they will eventually decay to  $(1, 0)$  mode EW gauge bosons/quarks along with SM quarks. The former decay, in turn, producing more stable SM particles like leptons, photons and quarks. Finally, the decay cascade terminates at the production of  $B_H^{(1,0)}$ , the first scalar excitation of the  $U(1)$  gauge boson. This, being the lightest  $(1, 0)$  mode particle, cannot decay further due to the conservation of KK-parity. So, in general, production of  $(1, 0)$  mode strongly interacting particles at the LHC will be characterised by the presence of number of leptons/jets/photons in association with transverse missing energy due to the weakly interacting  $B_H^{(1,0)}$ . In this article, we will be interested in a particular signature of this type, namely,  $n$ -jets (with  $n \geq 4$ ) + single photon + missing transverse energy. The somewhat complementary signal comprising of multi-leptons plus missing energy at the LHC as well as at the ILC has been investigated in Ref. [22].

The plan of the present article is as following. In section 2, we will discuss the 2UED model in general and particularly the SM in  $1 + 5$  dimensions. Section 3 will be devoted to the phenomenology of the  $(1, 0)$ -level of this model. In the next section, we will present our main result, i.e., the search strategies at the LHC operating with a center of mass energy of 7 and 14 TeV. Finally, we conclude in section 5.

## 2 Two Universal Extra Dimensions

In this section, we will briefly introduce the 2UED model, wherein all the SM fields can propagate universally in the  $(1 + 3 + 2)$ -dimensional space-time. With  $x^\mu$  ( $\mu = 0, 1, 2, 3$ ) denoting the Minkowski space, the compactification of the two extra dimensions can be described as follows:

- The flat extra dimensional space (before orbifolding) is a square with sides  $L$ , viz.

$0 \leq x^4, x^5 \leq L$  [11, 12]<sup>2</sup>. Identifying the opposite sides of the square would make the compactified manifold a torus. However, toroidal compactification leads to 4D fermions that are vector-like with respect to any gauge symmetry. The alternative is to identify two pairs of adjacent sides of the square [11, 12], namely,

$$(y, 0) \equiv (0, y), \quad (y, L) \equiv (L, y), \quad \forall y \in [0, L] . \quad (1)$$

This is equivalent to folding the square along a diagonal and glueing the boundaries. The above mechanism automatically leaves at most a single 4D fermion of a given chirality as the zero mode of any chiral 6D fermion [12].

- Clearly, the identification of Eq. (1) is valid only if, for any pair of identified points, the Lagrangian assumes identical value for any field configuration, viz.

$$\mathcal{L}|_{x^\mu, y, 0} = \mathcal{L}|_{x^\mu, 0, y}; \quad \mathcal{L}|_{x^\mu, y, L} = \mathcal{L}|_{x^\mu, L, y} .$$

This requirement fixes the boundary conditions for 6D scalar fields and Weyl fermions. While the gauge kinetic term allows for a two-fold ambiguity, the requirement that the boundary conditions for 6D scalar or fermionic fields be compatible with the gauge symmetry also fixes the boundary conditions for 6D gauge fields.

- Any 6D field (fermion/gauge or scalar)  $\Phi(x^\mu, x^4, x^5)$  can be decomposed as

$$\Phi(x^\mu, x^4, x^5) = \frac{1}{L} \sum_{j,k} f_n^{(j,k)}(x^4, x^5) \Phi^{(j,k)}(x^\mu), \quad (2)$$

where,

$$f_n^{(j,k)}(x^4, x^5) = \frac{1}{1 + \delta_{j,0} \delta_{k,0}} \left[ e^{-in\pi/2} \cos\left(\frac{jx^4 + kx^5}{R} + \frac{n\pi}{2}\right) + \cos\left(\frac{kx^4 - jx^5}{R} + \frac{n\pi}{2}\right) \right], \quad (3)$$

with the compactification radius  $R \equiv L/\pi$ . The 4D fields  $\Phi^{(j,k)}(x^\mu)$  are the  $(j, k)$ -th KK-modes of the 6D field  $\Phi(x^\alpha)$  and  $n$  is an integer whose value is restricted to 0, 1, 2 or 3 by the boundary conditions.

---

<sup>2</sup>In accordance with Refs. [11, 12], we have chosen the size of the extra dimensions to be the same. However, the most general case would imply two different sizes for these two directions. In absence of any obvious symmetry that relates these two length scales, we are thus considering only a specific choice.

- The functions  $f_n^{(j,k)}(x^4, x^5)$  should form a complete set on the compactified manifold, and, thus, must satisfy

$$\frac{1}{L^2} \sum_{j,k} [f_n^{(j,k)}(x^4, x^5)]^* f_n^{(j,k)}(x'^4, x'^5) = \delta(x'^4 - x^4) \delta(x'^5 - x^5). \quad (4)$$

It is clear from the form of  $f_n^{(j,k)}$  that the functions  $f_n^{(1,0)}$  and  $f_n^{(0,1)}$  are not independent ( $f_n^{(0,1)} = (-1)^n f_n^{(1,0)}$ ). Therefore, it is sufficient to take the set ( $j > 0, k \geq 0$ ) along with  $j = k = 0$  to form a complete set of functions on the chiral square. It is also obvious from the form of  $f_n^{(j,k)}(x^4, x^5)$  that only  $n = 0$  allows zero mode ( $j = k = 0$ ) fields in the 4D effective theory. The zero mode fields and the interactions among zero modes can be identified with the SM.

- In 6D, the Clifford algebra is generated by six anticommuting matrices,  $\Gamma^\alpha$ ,  $\alpha = 0, 1, \dots, 5$ , with the minimum dimensionality of the matrices being  $8 \times 8$ . Akin to 4D, the spinor representation of the  $SO(1, 5)$  Lorentz symmetry is reducible and contains two irreducible Weyl representation characterized by different eigenvalues of the 6D chirality operator  $\bar{\Gamma} \equiv \Gamma^0 \Gamma^1 \Gamma^2 \Gamma^3 \Gamma^4 \Gamma^5$ . The chirality projection operators are defined as  $P_\pm = (1 \pm \bar{\Gamma})/2$ , where  $+$  and  $-$  label the 6D chiralities defined by the eigenvalues of  $\bar{\Gamma}$ , viz.

$$\Psi_\pm(x^\alpha) = P_\pm \Psi(x^\alpha), \quad \bar{\Gamma} \Psi_\pm(x^\alpha) = \pm \Psi_\pm(x^\alpha). \quad (5)$$

The chiral fermions in 6D have four components. Each 6D chiral fermion contains both the chiralities of  $SO(1, 3)$ .

## 2.1 Introduction to the SM in 6D (6DSM)

Now we move on to the Standard Model in 6-dimensions. In 6D, the fields and boundary conditions are chosen such that, upon compactification and orbifolding, the zero modes of the resulting effective theory reproduce the SM. The requirements of anomaly cancellation and fermion mass generation force the weak-doublet fermions to have opposite *6D chiralities* with respect to the weak-singlet fermions. So the quarks of one generation are given by  $Q_+ \equiv (U_+, D_+)$ ,  $U_-$ ,  $D_-$ . Since observed quarks and leptons have definite 4D chirality, an immediate constraint is imposed on the boundary conditions of doublet and singlet fermions. The 6D doublet quarks and leptons decompose into a double tower of heavy vector-like 4D fermion doublets with left-handed zero mode doublets. Similarly, each 6D singlet quark and

lepton decomposes into towers of heavy 4D vector-like singlet fermions along with zero mode right-handed singlets. The zero mode fields are identified with the SM fermions. For example, SM doublet and singlets of 1st generation quarks are given by  $(u_L, d_L) \equiv Q_{+L}^{(0,0)}(x^\mu)$ ,  $u_R \equiv U_{-R}^{(0,0)}(x^\mu)$  and  $d_R \equiv D_{-R}^{(0,0)}(x^\mu)$ .

A given gauge field  $A_\alpha$  ( $\alpha = 0, 1 \dots 5$ ), on compactification, decomposes into a tower of 4D spin-1 field, with each of the two additional degrees of freedom *viz.*  $A_4$  and  $A_5$  giving rise to an additional tower of 4D spin-0 fields. One combination of the latter is eaten by the former to yield heavy spin-1 fields. The other combination remains in the physical spectrum as a tower of *spinless adjoints*. For example, the 6D gluon fields,  $G_\alpha^a$  decompose into a tower of 4D spin-1 fields,  $G_\mu^{a(j,k)}$ , and a tower of spin-0 fields,  $G_H^{a(j,k)}$ , with the former including a zero mode to be identified with the SM gluon. Similarly, the 6D  $SU(2)$  gauge fields have KK-modes  $W_\mu^{(j,k)\pm}$ ,  $W_H^{(j,k)\pm}$ ,  $W_\mu^{(j,k)3}$  and  $W_H^{(j,k)3}$ , while the hypercharge gauge field has KK-modes  $B_\mu^{(j,k)}$  and  $B_H^{(j,k)}$ . The zero modes of  $W_\mu^{(j,k)\pm}$  towers are identified with the SM  $W_\mu^\pm$  bosons. The mixing of  $W_\mu^{(0,0)3}$  and  $B_\mu^{(0,0)}$  gives the photon and the  $Z$ -boson. For non-zero modes this mixing is negligible, though.

The tree-level masses for  $(j, k)$ -th KK-mode particles are given by  $\sqrt{M_{j,k}^2 + m_0^2}$ , where  $M_{j,k}^2 \equiv (j^2 + k^2)/R^2$  and  $m_0$  is the mass of the corresponding zero mode particle. As a result, for sufficiently large  $R^{-1}$  (as demanded by phenomenological consistency), the tree-level masses are approximately degenerate within a given non-trivial KK level. This degeneracy is lifted by radiative effects [23]. The fermions receive mass corrections from the gauge interactions (with gauge bosons and spinless adjoints) as well as Yukawa interactions, with each contributing a positive mass shift.

The gauge fields and spinless adjoints receive mass corrections from the self-interactions and gauge interactions. While the fermion loops (via gauge interactions) lead to negative mass shifts, self-interactions give positive shifts. The latter are, of course, nonexistent for the  $B_\mu^{(j,k)}$  and for the corresponding scalars  $B_H^{(j,k)}$ . Explicit computations show that the lightest KK particle is the spinless adjoint  $B_H^{(1,0)}$ . As a result, the 2UED model gives rise to a scalar dark matter [15]. Consistency of the relic abundance of the  $B_H^{(1,0)}$  with  $\Omega_{DM}$  as inferred from WMAP observations [24] leads to a very constrained allowed region in the  $R$ - $m_{\text{higgs}}$  plane, confined to  $R^{-1} \lesssim 500 \text{ GeV}$ . However, note that the analysis of Ref. [15] was performed only at the leading order and higher order corrections would, typically, be expected to increase the annihilation cross-sections and, thereby, push up the allowed range

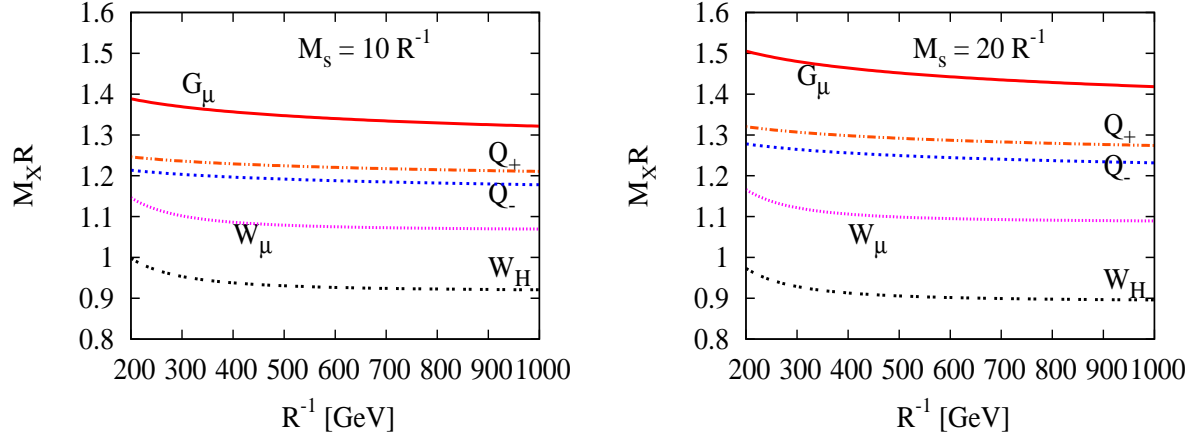


Figure 1: Variation of  $M_X R$  (where  $X$  corresponds to either  $G_\mu^{(1,0)}$ ,  $Q_+^{(1,0)}$ ,  $Q_-^{(1,0)}$ ,  $W_\mu^{(1,0)}$  or  $W_H^{(1,0)}$ ) as a function of  $R^{-1}$  for two different values of  $M_s R$ . Here,  $Q_\pm^{(1,0)}$  does not include the top's partners.

in  $R^{-1}$ . Much more importantly, the inclusion of the higher KK modes in the annihilation (as well as co-annihilation) of the DM candidate significantly raises the  $R^{-1}$  range, as has recently been demonstrated [10] for the mUED case. In the current context, this effect is expected to be even stronger. Consequently, we shall not impose the WMAP constraint on the maximum allowed value for  $R^{-1}$ .

### 3 Phenomenology of $(1, 0)$ -mode sector of 6DSM

In the preceding section, we identified the standard model doublet and singlet quarks with the  $(0, 0)$  modes of the 6D fields  $Q_+$ ,  $U_-$  and  $D_-$  respectively. Similar would be the case for the leptonic fields. The  $(1, 0)$ -mode fermionic sector thus constitutes of  $Q_+^{(1,0)}$ ,  $U_-^{(1,0)}$ ,  $D_-^{(1,0)}$ ,  $L_+^{(1,0)}$  and  $E_-^{(1,0)}$ . As for the corresponding bosonic sector, we have, apart from the Higgs (scalar) and gauge boson (vector) excitations, another set of three scalars transforming under the adjoint representation of the respective gauge groups. The last mentioned, for which there is no analog in the mUED case, would play a key role.

While the tree-level masses, in the absence of electroweak symmetry breaking, would be  $R^{-1}$  for each, the inclusion of radiative corrections does change them [23]. With the change being dependent on the cutoff scale  $M_s$  (note that a ultraviolet completion needs to be defined for all such theories), we present the corrections for  $M_s = 10$  (20) $R^{-1}$ . To be

specific,

$$\begin{aligned}
M_{L_+} &\simeq 1.04(1.06) R^{-1}, & M_{E_-} &\simeq 1.0(1.0)R^{-1}, \\
M_{B_\mu} &\simeq 0.97(0.96) R^{-1}, & M_{B_H} &\simeq 0.86(0.82) R^{-1}, \\
M_{G_H} &\simeq 1.0(1.0) R^{-1}, & &
\end{aligned} \tag{6}$$

with the numerical factors being almost independent of  $R^{-1}$ . For the other colored states, an additional mild dependence accrues from the scale dependence of the QCD coupling constant. For the  $SU(2)$  gauge bosons and spinless adjoints, the  $R^{-1}$  dependence arises from the non-zero mass of the SM  $W^\pm$  and  $Z$ -boson. In Fig. 1, we present these masses as a function of  $R^{-1}$  with  $\alpha_s = \alpha_s(M_X)$ . It should be noted that a smaller  $M_s R$  leads to a more degenerate spectrum, and, consequently, in the collider context, a more difficult situation to explore.

### 3.1 Decay of $(1, 0)$ -mode particles

Decays of the  $(1, 0)$ -mode particles have been investigated in detail in Ref. [17]. Conservation of KK-parity allows  $(1, 0)$ -mode particles to decay only into a  $(1, 0)$ -mode particle and one or more SM particles if kinematically allowed. It is clear from Eq. (6) that  $B_H^{(1,0)}$  is the lightest KK particle (LKP) in this theory. It is important to notice that, unlike the case of the mUED, the LKP is now a scalar. Since the  $B_H^{(1,0)}$  is a stable particle and weakly interacting, it passes through the detector without being detected. Decays of all the  $(1, 0)$ -mode particles thus result in one or more SM particles plus missing energy/momentum signature. We briefly discuss below the decays of the different  $(1, 0)$ -mode particles. Unless specified, we shall, henceforth, limit ourselves to  $300 \text{ GeV} \leq R^{-1} < 1 \text{ TeV}$  and  $M_s = 10 R^{-1}$ . Furthermore, we shall neglect the production of  $T_{+,-}^{(1,0)}$ , the partners of the top quarks.

- **$(1, 0)$ -mode gluons ( $G_\mu^{(1,0)}$ )**: The heaviest of the  $(1, 0)$ -mode particles, the  $G_\mu^{(1,0)}$  has tree-level gauge couplings with a SM quark and the corresponding  $(1, 0)$ -mode quark. The decay of  $G_\mu^{(1,0)}$  into  $Q_-^{(1,0)}$  is slightly favoured by phase space. The branching fractions of  $G_\mu^{(1,0)}$  into a quark plus  $Q_+^{(1,0)i}$ ,  $U_-^{(1,0)i}$ , or  $D_-^{(1,0)i}$ , summed over the index  $i$  which labels the three generations, are 36.7%, 24.6% and 38.7%, respectively. It is important to note that, for  $1/R \leq 1.3 \text{ TeV}$ , the decays of the  $(1, 0)$  vector gluon into  $t_L T_+^{(1,0)}$  or  $t_R T_-^{(1,0)}$  are kinematically forbidden.



- **(1,0)-mode quarks ( $Q_+^{(1,0)}$  and  $Q_-^{(1,0)}$ )**: These are heavier than the (1,0)-mode electroweak gauge bosons and all of the spinless adjoints, and can, thus, decay into either, accompanied by a quark. Understandably, the decay to the  $SU(3)$ -spinless adjoint (driven by QCD) is the dominant one for both doublet and singlet (1,0)-mode quarks. The  $SU(2)_W$  doublet (1,0) quarks can also decay into a SM quark, and an  $SU(2)_W$  gauge boson or spinless adjoint. Both doublet and singlet (1,0)-mode quarks may also decay into (1,0)-mode hypercharge bosons or spinless adjoints. The branching fractions of  $Q_+^{(1,0)}$  into  $qG_H^{(1,0)}$ ,  $qW_H^{(1,0)3}(W_H^{(1,0)+})$  and  $qW_\mu^{(1,0)3}(W_\mu^{(1,0)+})$  are given by 63.2%, 5.6%(11.2%) and 6.4%(12.8%) respectively. The decay of the doublet quarks into  $qB_H^{(1,0)}(B_\mu^{(1,0)})$  is suppressed by the hypercharge. The branching fractions of  $Q_-^{(1,0)}$  into  $q_R G_H^{(1,0)}$  and  $q_R B_\mu^{(1,0)}(B_H^{(1,0)})$  are given by 82.1% and 11.5%(6.4%) respectively for the up type quarks ( $U_-^{(1,0)}$ ) and 94.8% and 3.3%(1.9%) respectively for the down type quarks ( $D_-^{(1,0)}$ ).
- **$SU(3)_C$  spinless adjoint ( $G_H^{(1,0)}$ )**: This suffers a tree-level 3-body decay into a  $q\bar{q}$  pair plus one of the electroweak (1,0)-mode gauge boson or spinless adjoint. The dominant mode is  $G_H^{(1,0)} \rightarrow B_H^{(1,0)} q\bar{q}$ , with a total branching fraction of 96.5%. The other decay modes (into electroweak gauge bosons and spinless adjoints) are suppressed by the small mass splitting between them and the  $G_H^{(1,0)}$ .
- **$SU(2)$  gauge bosons ( $W_\mu^{(1,0)\pm}$  and  $W_\mu^{(1,0)3}$ )**: Since these are heavier than the (1,0)-mode leptons, they decay dominantly into the doublet fields. For example,  $W_\mu^{(1,0)3}$  can decay into one of the six ( $l_i L_{+i}^{(1,0)}$  and  $\nu_i \nu_{+i}^{(1,0)}$ ,  $i = e, \mu, \tau$ ) channels with equal probability. Similarly,  $W_\mu^{(1,0)\pm}$  decays into one of the six possible modes ( $l_i \nu_{+i}^{(1,0)}$  and  $\nu_i L_{+i}^{(1,0)}$ ,  $i = e, \mu, \tau$ ) with a branching fraction of 1/6 into each.
- **(1,0)-mode leptons ( $L_+^{(1,0)}$  and  $E_-^{(1,0)}$ )**: Being heavier than  $B_\mu^{(1,0)}$ ,  $B_H^{(1,0)}$  and  $SU(2)$  spinless adjoints, they can decay into the latter and the corresponding lepton.
- **$U(1)$  gauge boson ( $B_\mu^{(1,0)}$ )**: It has a tree level 3-body decay into a pair of SM fermions and the  $B_H^{(1,0)}$ . Being driven by the hypercharge, the decay into the right-handed leptons dominates that into the doublet fermions. Since the corresponding (1,0) fermion appears in the propagator, the decays into quarks (e.g.,  $B_\mu^{(1,0)} \rightarrow u_R \bar{u}_R B_H^{(1,0)}$ ) suffer a further suppression on account of the largeness of the propagator mass. On the other hand, the one-loop decay  $B_\mu^{(1,0)} \rightarrow \gamma B_H^{(1,0)}$  amplitude receives contribution from each of the fermion species as well as the Higgs. While this amplitude would have vanished in

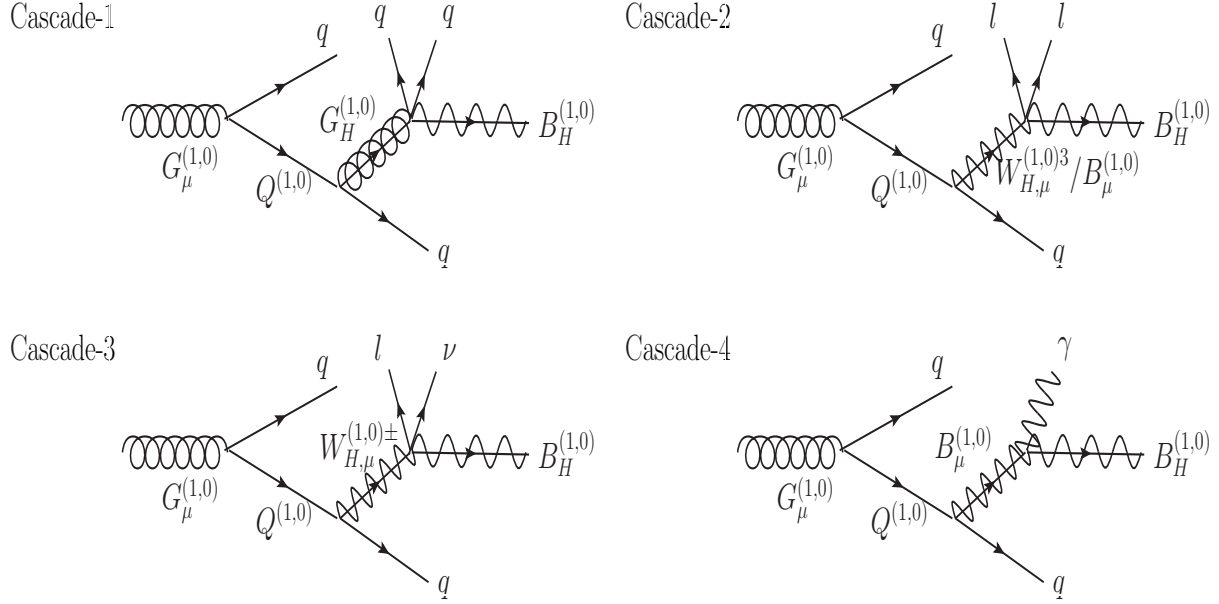


Figure 2: Decay cascades of  $G_\mu^{(1,0)}$ .

the limit of all the  $(1, 0)$  fermionic fields being degenerate, the split described above is sufficient to render it quite substantial. Indeed, the dominant modes are  $B_\mu^{(1,0)}$  in  $\bar{l}lB_H^{(1,0)}$  (where  $l$  includes  $e$ ,  $\mu$  and  $\tau$ ) and  $\gamma B_H^{(1,0)}$  with the respective branching fractions, for  $R^{-1} = 500$  GeV, being 63.5% and 36.2%.

- $SU(2)$  spinless adjoints ( $W_H^{(1,0)\pm}$  and  $W_H^{(1,0)3}$ ): These can decay only to the  $B_H$  and SM particles [20]. The  $W_H^{(1,0)3}$  decays to a pair of SM leptons and  $B_H^{(1,0)}$  with equal branching ratio to charged leptons and neutrinos. Branching fraction to quark antiquark pairs is again negligible due to hypercharge and heavy  $(1, 0)$ -mode quark propagator. The  $W_H^{(1,0)\pm}$ , on the other hand, decay with almost 100% branching ratio to  $l\bar{\nu}_l B_H^{(1,0)}$  ( $l$  includes all 3 SM lepton generations). Branching fractions of  $SU(2)$  spinless adjoints are essentially independent of  $R^{-1}$ .

We are now equipped enough to discuss the decay cascade of the strongly interacting  $(1, 0)$ -mode particles. Let us first begin with the  $G_\mu^{(1,0)}$ , which decays into a SM quark and the corresponding  $(1, 0)$ -mode quarks. The latter decays into the spinless adjoints or electroweak gauge bosons in association with a SM quark. The decay of  $Q_-^{(1,0)}$  into  $G_H^{(1,0)}$  results in four SM quarks plus  $B_H^{(1,0)}$  in the final state, whereas the decay into  $SU(2)$  gauge bosons or spinless adjoints gives rise to two SM quarks and two SM leptons in association with a

$B_H^{(1,0)}$ . However, there is one more interesting decay mode available, namely  $Q_-^{(1,0)} \rightarrow qB_\mu^{(1,0)}$ , which gives rise to two SM quark + one photon + a  $B_H^{(1,0)}$  at the end of a single  $G_\mu^{(1,0)}$  decay cascade. The decay cascades of  $G_\mu^{(1,0)}$  are schematically shown in Fig. 2.

### 3.2 Production cross sections

Owing to KK-parity, the  $(1, 0)$  mode particles can only be pair-produced. We shall restrict ourselves only to the production of strongly interacting  $(1, 0)$ -mode particles as the cross-sections for the color-singlet states are suppressed by more than an order of magnitude.

All the  $(1, 0)$ -mode gauge bosons and spinless adjoints have tree level couplings with an  $(1, 0)$ -mode fermion and a SM fermion arising from the compactification of the 6D kinetic term for fermions. Similarly, the compactification of the kinetic term for the 6D gluon field gives rise to both  $G_{\mu/H}G_{\mu/H}g$  and  $G_{\mu/H}G_{\mu/H}gg$  couplings. Thus,  $GG$  production will proceed from both the  $gg$  initial state (by virtue of the aforementioned couplings) as well as from a  $q\bar{q}$  initial state (through a  $s$ -channel SM gluon). Owing to the larger mass of the  $G$ , this particular mode never dominates though. What does, for a significant part of the parameter space, is  $QG$  production which proceeds from the initial  $qg$  state through a combination of three Feynman diagrams (a  $s$ -channel  $q$ , a  $t$ -channel  $Q$  and a  $u$ -channel  $G$ ). Also of particular interest is  $q_iq_j \rightarrow Q_iQ_j$  production that proceeds through  $t/u$ -channel  $G$  exchange. Given that the LHC is a  $pp$  machine, this would be expected to dominate for large  $R^{-1}$ .

While the electroweak diagrams would also contribute to the last-mentioned (as well as to  $Q_i\bar{Q}_j$  production), these amplitudes are suppressed by a relative factor of  $(\alpha_{EW}/\alpha_s)$ . And given that they do not bring in any new topologies, their total contribution is rather subdominant.

Finally, the processes of interest are

$$pp \implies G_\mu + G_\mu, \quad G_\mu + Q_i, \quad Q_i + Q_j, \quad Q_i + \bar{Q}_j, \quad (7)$$

where the indices  $i, j$  run over both flavour and the 6D chirality. In Fig. 3, we show the total cross sections for some of these modes at the LHC, obtained using the CTEQ6L parton distribution functions [25, 26] with the factorization scale fixed at  $Q^2 = \hat{s}/4$  (for  $300 \text{ GeV} \leq R^{-1} \leq 1000 \text{ GeV}$ ). While there exists a dependence on these two choices, we are not, by any means, overestimating the signal size. In the absence of any computation of the higher order corrections (expected only to enhance these numbers), we limit ourselves to only tree-level

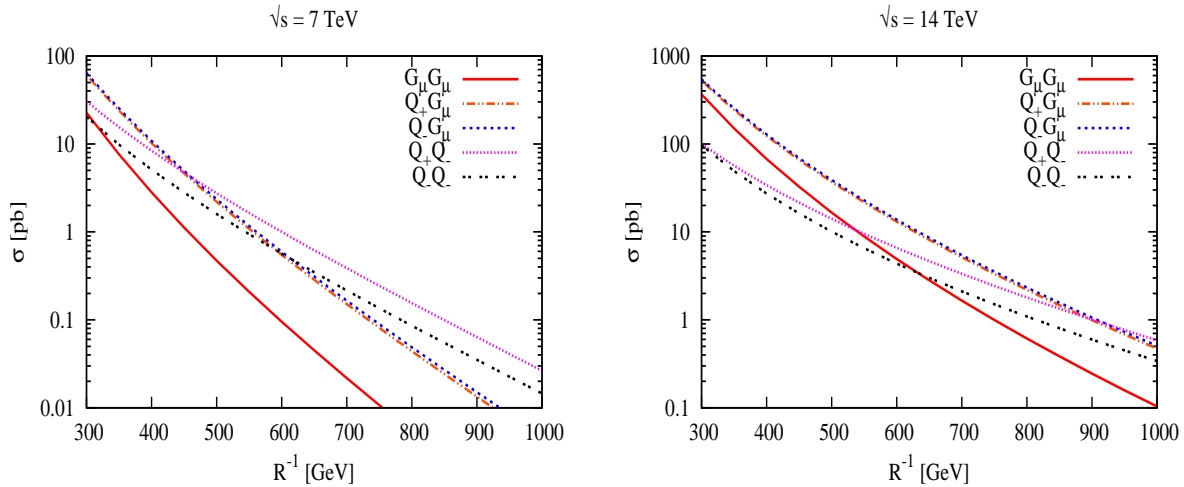


Figure 3: Total pair production cross-sections of  $(1, 0)$ -mode particles at the LHC operating with  $\sqrt{s} = 7$  TeV (left), and 14 TeV (right).

calculations.

## 4 Signature of 6DSM at the LHC

In general, pair production of coloured  $(1, 0)$ -mode particles— depending upon the decay chain—can give rise to  $n$ -jet+ $m$ -lepton+ $\ell$ -photon+ $\cancel{p}_T$  signatures. For example, pair production of the  $SU(3)_C$  gauge boson  $G_\mu$ , followed by its hadronic decay, leads to 8 partons accompanied by missing- $\cancel{p}_T$ , with each parton potentially leading to one jet (or more). However, the multi-jet+ $\cancel{p}_T$  signature is expected to be overwhelmed by the pure QCD background<sup>3</sup>, and we shall desist from using it any further.

Multi-jet+multi-lepton+ $\cancel{p}_T$  results when one  $G_\mu$  follows the decay “Cascade-1” of Fig. 2 and other follows either of “Cascade-2” and “Cascade-3”. It has been shown in Ref. [28] that this signature can serve as a potential discovery channel for the mUED model. In principle, one could perform a similar kind of analysis in the context of  $6DSM$  as well. However, the presence of  $G_H^{(1,0)}$  in the particle spectrum significantly reduces the leptonic branching fractions for the excited quarks and gluons when compared to the mUED.

---

<sup>3</sup>Although Ref. [27] has claimed, in a different context, that such a final state can be used, it requires very sophisticated handling and the robustness of the stratagem developed therein is yet to be vindicated.

Instead, we consider the final state

$$n\text{-jets} + \gamma + \cancel{p}_T \quad (n \geq 4) \quad (8)$$

where the hard photon will be used as an additional trigger. The main motivations for choosing this particular signal topology are two fold. First of all, this signature serves to distinguish between the 2UED and mUED models. The particle spectrum of the mUED model does not contain the spinless adjoints. Hence, the first KK-excitation of the  $U(1)$  gauge boson is the LKP therein, and its further decay is not possible. The second reason is of course the rate of the SM background, which is reduced substantially with the emission of an isolated hard photon in the multi-jet events. In the 2UED model, such a final state topology arises when one  $G_\mu$  decays hadronically and the other one follows the ‘‘Cascade-4’’ decay chain.

Several SM processes constitute potential backgrounds for the signal of Eq.(8) and we now discuss the dominant ones in succession.

- An irreducible background arises from the production of a  $Z$ -boson in association with a *photon* and multiple jets. The  $Z$ -boson decays invisibly and gives rise to the missing transverse energy signature:

$$pp \rightarrow Z + \gamma + n\text{-jets} \rightarrow \nu\bar{\nu} + \gamma + n\text{-jets} \quad (9)$$

We use the ALPGEN [29] generator to estimate the background contribution originating from the above SM process. Although the total cross section for this process is very large, the imposition of sufficiently strong  $p_T$  and rapidity requirements on the photon and the jets serves to suppress it strongly. In particular, the radiation of every additional hard (and well-separated) jet would, typically, cost an additional factor of  $\alpha_s$ . However, since ours will not be a very sophisticated analysis, it is quite conceivable that we might underestimate the background, especially where jet reconstruction is concerned. To compensate for this, we will include even ostensible 3-jet events in the background while requiring  $n \geq 4$  for the background.

- The production of  $W^\pm$  in association with a photon and multiple jets can also be a possible source of background, if the  $W^\pm$  decays leptonically and the charged lepton is missed somehow. To be specific, we consider it to be undetectable if it either falls outside the rapidity coverage ( $|\eta| \geq 2.5$ ) or if it is too soft ( $p_T \leq 10$  GeV) or if it lies

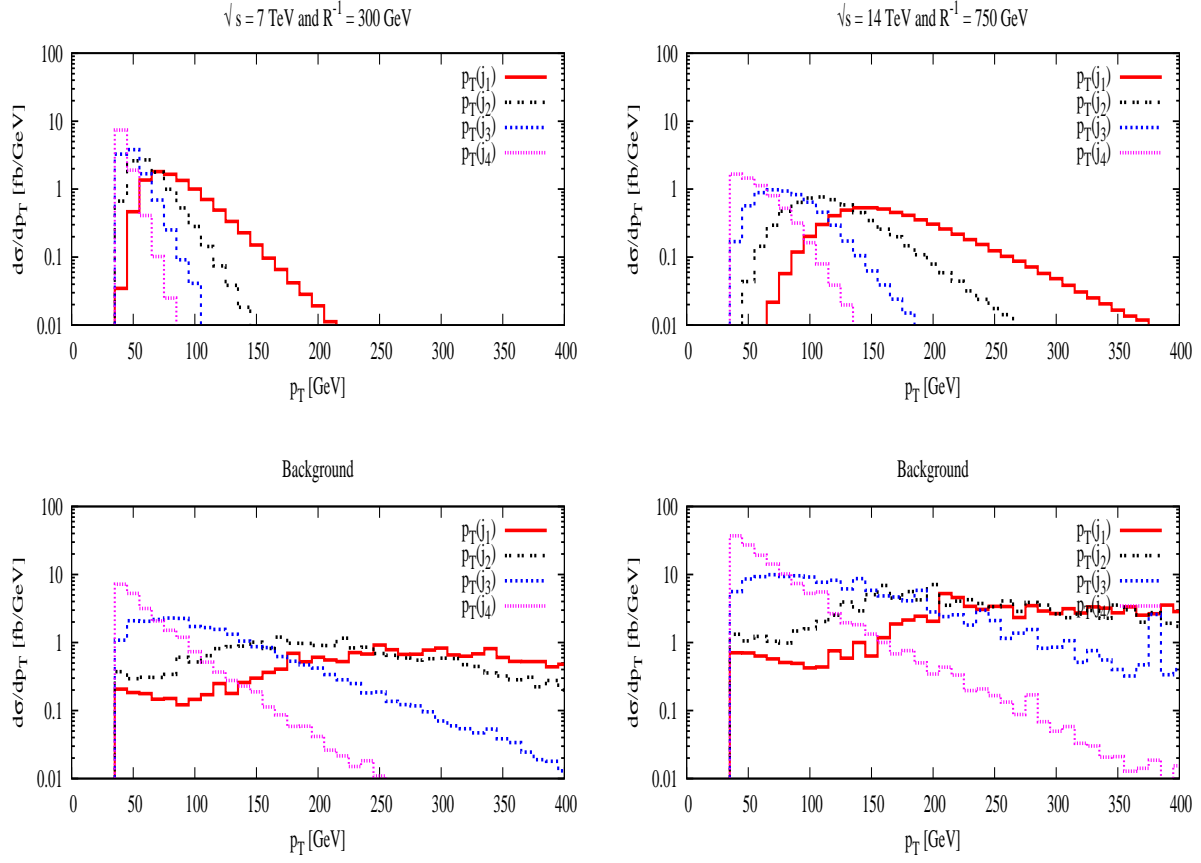


Figure 4: Transverse momentum distribution of jets (after ordering them according to their  $p_T$  hardness) after the acceptance cuts for both signal (top panel) and the SM background (bottom panel) at the LHC with  $\sqrt{s} = 7$  TeV (left), and 14 TeV (right).

too close to any of the jets. In this case, the neutrino and the missing lepton together give rise to the missing transverse momentum. This background too we estimate using ALPGEN. Given the fact that the  $W$  has a substantial mass and that it is produced with relatively low rapidity, it stands to reason that the charged lepton would, most often, be well within the detector and also have sufficient  $p_T$  to be detectable. Consequently, the probability of missing the charged lepton is small, and this background would be suppressed considerably. Indeed, this is borne out by actual computation.

- Significant background contribution can come from the production of a *photon* in association with four or more jets.

$$pp \rightarrow \gamma + nj \quad \text{with} \quad n \geq 4 \quad (10)$$

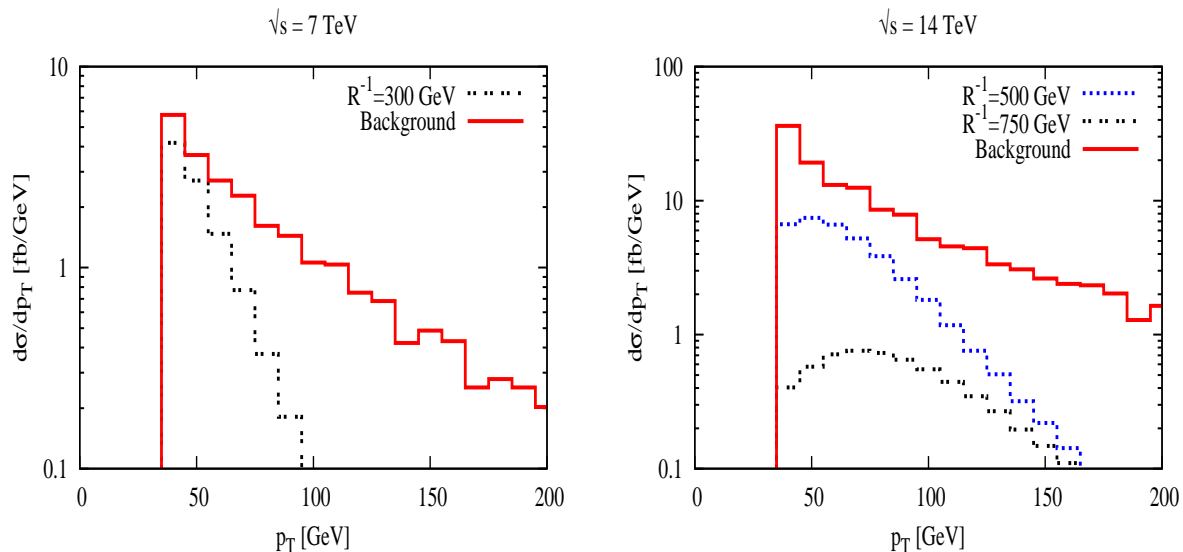


Figure 5: Photon  $p_T$  distributions after the *acceptance cuts* for both signal and the SM background at the LHC with  $\sqrt{s} = 7$  TeV (left), and 14 TeV (right).

In this case, there is no real source of missing transverse momentum. However, mis-measurement of the  $p_T$  of jets and photon can lead to some amount of missing transverse momentum. Since the cross section for the aforementioned process is large, this process, in principle, could contribute significantly to the background.

- Top anti-top ( $t\bar{t}$ ) pair production in association with a photon is another source:

$$pp \rightarrow t\bar{t} \gamma. \quad (11)$$

Hadronic decay of the  $t\bar{t}$  pair could lead to a final state comprising of, say, 6 jets alongwith a photon. The missing  $p_T$  would result from the mis-measurement of the jets and photon momentum. Similarly, the semi-leptonic decay of the  $t\bar{t}$  pairs ( $pp \rightarrow t\bar{t}\gamma \rightarrow 4q + \gamma + l + \nu$ ) also contributes to the background if the charged lepton is missed. In this case, the neutrino momentum would add to the contribution from the mismeasurement to yield the total missing  $p_T$ .

- Single top (in association with a quark or a  $W$ ) production, although an electroweak process, has a production cross section at the LHC that is quite comparable to that for  $t\bar{t}$ . Radiating off a photon (as in  $pp \rightarrow t + \gamma + X$  with  $X$  not being a top) would, naively, result in a background that is suppressed compared to that from  $t\bar{t}\gamma$  by a factor

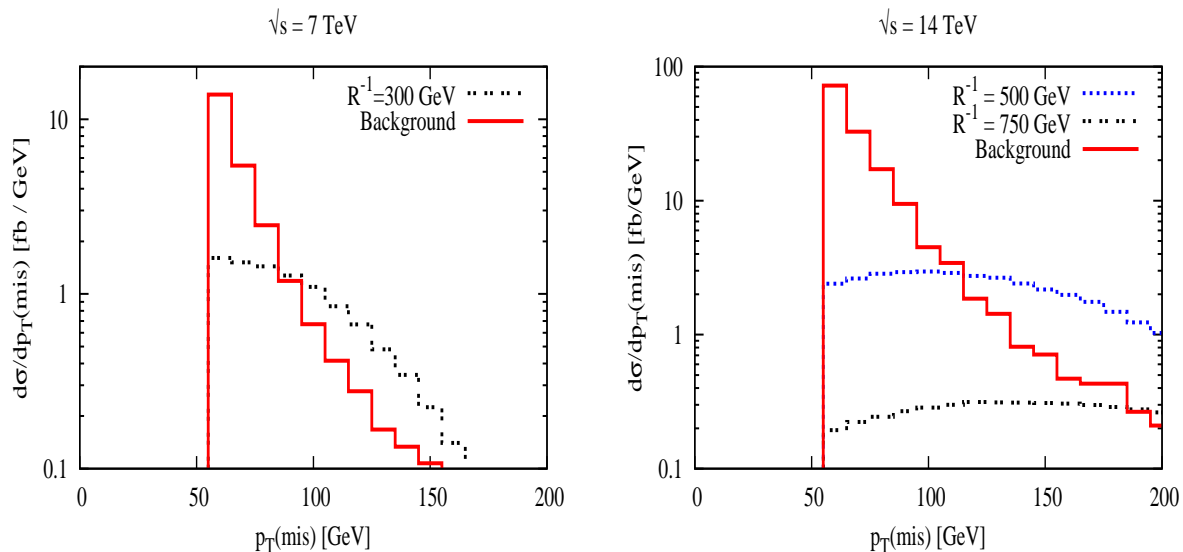


Figure 6: Missing transverse momentum distributions after the acceptance cuts for both signal and the SM background at the LHC with  $\sqrt{s} = 7$  TeV (left), and 14 TeV (right).

$\sim \sigma(t + X)/\sigma(t\bar{t})$ . However, note that, for a very large fraction of these events,  $X$  is a quark and produced preferentially with a low  $p_T$  and/or high rapidity. Such and other considerations turn this background quite subdominant.

- Also to be considered are events such as

$$pp \rightarrow W^\pm + n\text{-jets} \rightarrow e^\pm + \nu + n\text{-jets}.$$

If the  $e^\pm$  does not leave a track in the detector, then a hit in the electromagnetic calorimeter would qualify it as a photon, thereby mimicking the signal of Eq.(8). Pending a full detector simulation, an accurate estimate of this background is not possible. However, the probability of an  $e^\pm$  of  $p_T > 10$  GeV not leaving a track is very low [30]. As a result, this background is expected to be suppressed in comparison to that from  $(W^\pm + \gamma + n\text{-jets})$ -production despite the latter appearing only at a higher order of perturbation theory.

- Last, but not the least, is the pure QCD background, namely just  $n$ -jet production, with one jet faking a photon. With the rates for  $n$ -jet production being quite large, it is conceivable that this background could be substantial. Again, an accurate estimation would need a full detector simulation. However, as previous studies have shown, for



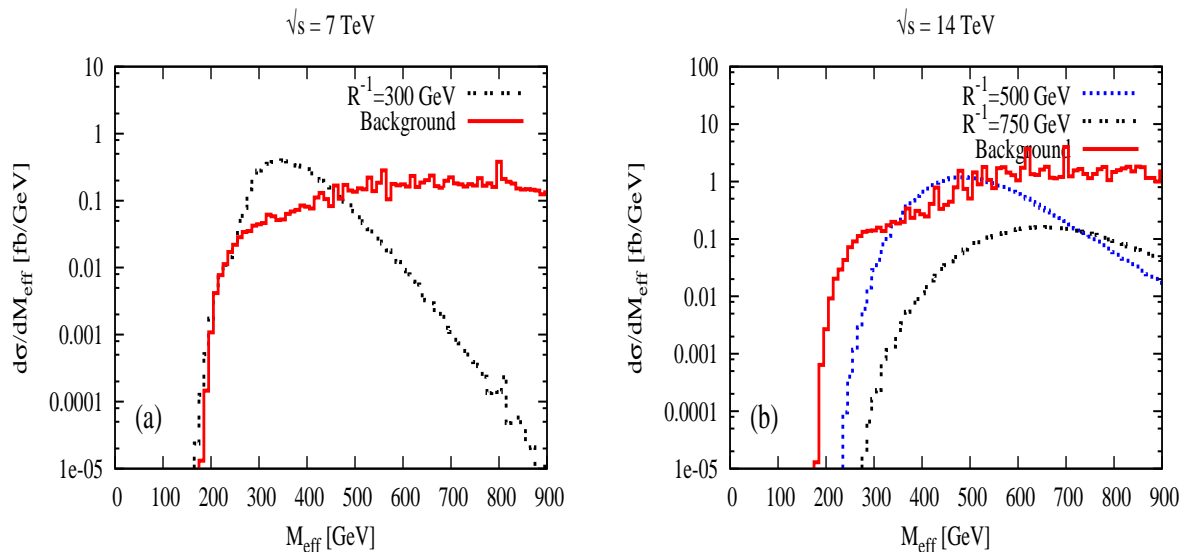


Figure 7: Effective mass distributions after the acceptance cuts for both signal and the SM background at the LHC with  $\sqrt{s} = 7$  TeV (left), and 14 TeV (right).

sufficiently high values of the minimum  $p_T$  required, the probability of photon faking is  $\sim 10^{-3}$ – $10^{-4}$ , and, once again, this background turns out to be smaller than that from  $\gamma + n$ -jets.

At this stage, we are equipped enough to develop a systematic methodology of suppressing the SM backgrounds without drastically reducing effecting the signal. A fruitful perusal of such a methodology requires that we carefully examine and compare the phase space distributions of different kinematic variables for signal as well as backgrounds discussed above. However, before we embark on the mission to suppress the aforementioned backgrounds, it is important to list a set of basic requirements for jets and photons to be visible at the detector. It should be appreciated that any realistic detector has only a finite resolution; this applies to both energy/transverse momentum measurements as well as the determination of the angle of motion. For our purpose, the latter effect can be safely neglected<sup>4</sup> and we simulate the former by smearing the energy with Gaussian functions. The energy resolution function receives contributions from many sources and are, in general, a function of the detector coordinates. We, though, choose to simplify the task by assuming a flat resolution

<sup>4</sup>The angular resolution is, generically, far superior to the energy/momentum resolutions and too fine to be of any consequence at the level of sophistication of this analysis.

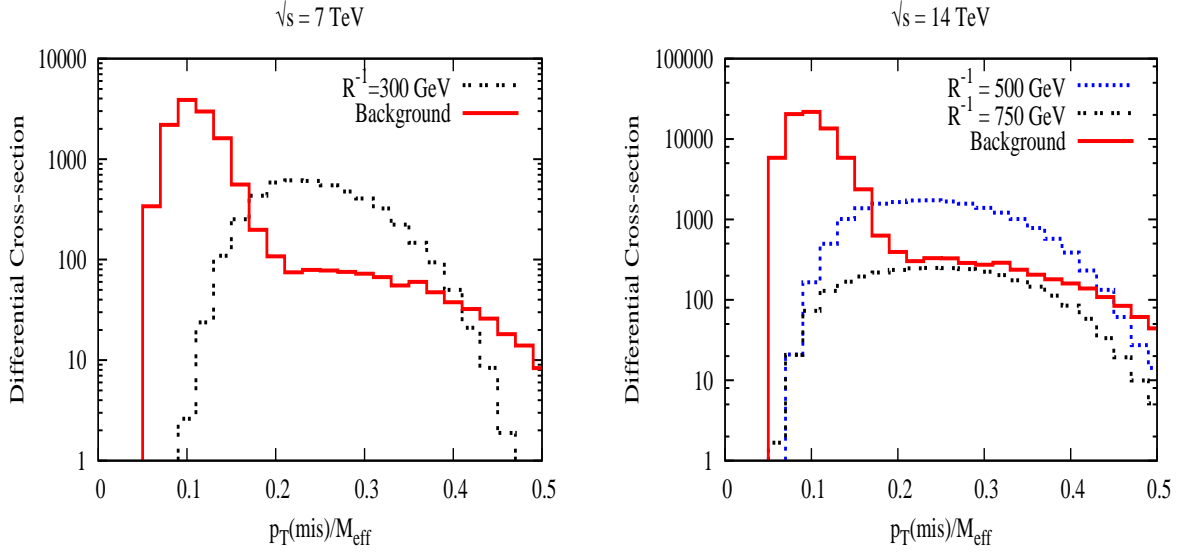


Figure 8: Distributions in the ratio  $p_T/M_{\text{eff}}$  after the acceptance cuts for both signal and the SM background at the LHC with  $\sqrt{s} = 7$  TeV (left) and 14 TeV (right).

function equating it to the worst applicable for our range of interest, namely,

$$\frac{\Delta E}{E} = \frac{a}{\sqrt{E/\text{GeV}}} \oplus b, \quad (12)$$

where,  $a_\ell = 5\%$ ,  $b_\ell = 0.55\%$  and  $a_j = 100\%$ ,  $b_j = 5\%$ , and  $\oplus$  denotes a sum in quadrature. Keeping in mind the LHC environment as well as the detector configurations, we demand that, to be visible, a jet or a photon must have an adequately large transverse momentum and they are well inside the rapidity coverage of the detector, namely,

$$p_T^j > 30 \text{ GeV}, \quad p_T^\gamma > 30 \text{ GeV}, \quad (13)$$

$$|\eta_j| \leq 2.5, \quad |\eta_\gamma| \leq 2.5. \quad (14)$$

We demand that both photon and jets be well separated so that they can be identified as individual entities. To this end, we use the well-known cone algorithm defined in terms of a cone angle  $\Delta R_{ij} \equiv \sqrt{(\Delta\phi_{ij})^2 + (\Delta\eta_{ij})^2}$ , with  $\Delta\phi$  and  $\Delta\eta$  being the azimuthal angular separation and rapidity difference between two particles. Quantitatively, we impose

$$\Delta R_{\gamma j} > 0.4 \text{ and } \Delta R_{jj} > 0.7. \quad (15)$$

Furthermore, the event must be characterized by a minimum missing transverse momentum defined in terms of the total visible momentum, namely,

$$\cancel{p}_T \equiv \sqrt{\left(\sum_{\text{vis.}} p_x\right)^2 + \left(\sum_{\text{vis.}} p_y\right)^2} > 50 \text{ GeV} . \quad (16)$$

It has been discussed already that for some of the SM backgrounds, the hard (parton level) process does not even have a source of missing energy. For example, the  $4j+\gamma$  final state could potentially be associated with a missing transverse momentum only on account of mismeasurements of the jets and photon energies. A minimum requirement of the missing transverse momentum keeps these backgrounds well under control. We also impose a lower bound on the *jet-jet* and *jet-photon* invariant mass.

$$M_{\gamma j} \geq 20 \text{ GeV} \text{ and } M_{jj} \geq 20 \text{ GeV} . \quad (17)$$

The last two cuts are aimed to avoid any collinear and soft singularities associated with the emission of a photon/gluon from a quark, while estimating the background processes, which we evaluate using LO matrix elements. The requirements summarised in Eqs. (13–17) constitute our *acceptance cuts*.

With the set of acceptance cuts and detector resolution defined in the previous paragraph, we compute the signal and background cross-sections at the LHC operating with  $\sqrt{s} = 7$  TeV and 14 TeV respectively and display them in Table 1. Clearly, the backgrounds are still large compared to the signal. The dominant SM background contribution arises from the production of a photon in association with jets<sup>5</sup>. In order to enhance the signal to background ratio, we study distributions of different kinematic observables.

In Fig. 4, we display the  $p_T$  distributions of the signal (top panels) and background (bottom panels) jets after ordering them according to their  $p_T$  ( $p_T^{j_1} > p_T^{j_2} > p_T^{j_3} > p_T^{j_4}$ ). From the shape of the  $p_T$  distributions in Fig. 4 it is very obvious that the signal jets are relatively softer than the background jets. The former result from the decay of excited gluons ( $G_\mu^{(1,0)}$ ) and quarks ( $Q_-^{(1,0)}$  and  $Q_+^{(1,0)}$ ) into other excited electroweak gauge bosons and spinless adjoints. With the relative mass splitting between the excited quarks/gluons and the weak gauge bosons and spinless adjoints being small, it is quite obvious that, in the rest frame of the primary produced particle, the daughter jets would carry only a small fraction

---

<sup>5</sup>Indeed, the dominance is strong enough to render inefficient the use of additional cuts such as ones on  $|M_{jj} - M_{Z/W}|$  to eliminate resonant  $Z/W$  production.

Cross-section in fb				
$\sqrt{s} = 7$ TeV		$\sqrt{s} = 14$ TeV		
$R^{-1}$ [GeV]	Background	$R^{-1}$ [GeV]		Background
300	cross-section	500	750	cross-section
98.6	252.5	376.3	62.1	1478.1

Table 1: Signal and SM background cross-sections (in fb) after the acceptance cuts for different values of  $\sqrt{s}$  and  $R^{-1}$ .

of its mass as momenta. This, in turn, translates to relatively small transverse momenta for them. This characteristic of the signal could, in principle, be exploited to enhance the signal to background ratio. However, while an upper bound on the jet  $p_T$  would suppress the SM backgrounds, it is important to notice that (see Fig. 4) the hardness of signal jet  $p_T$ s depends on the center-of-mass ( $\sqrt{s_{pp}}$ ) energy of the collider as well as on the compactification radius  $R$ . Thus, to suppress the SM background without reducing the signal, such an upper bound (if any), has to be designed keeping in mind both both  $\sqrt{s_{pp}}$  and  $R^{-1}$ . Similar is the situation with the photon  $p_T$  distribution (see Fig. 5). In Fig. 5, we show the  $p_T$  distributions for the signal and background photons for  $\sqrt{s} = 7$  TeV (left panel) and 14 TeV (right panel) of the LHC center of mass energy. Here too, a  $\sqrt{s_{pp}}$  and  $R^{-1}$  dependent upper bound on the photon transverse momentum would improve the signal to noise ratio. However, in absence of any information about  $R^{-1}$ , it is extremely challenging to introduce such a cut. Therefore, in our analysis, we do not use any further  $p_T$  cuts.

In Fig. 6, we display the missing transverse momentum distribution for the signal and background for two values of LHC center of mass energies. The background is peaked at a relatively low  $\cancel{p}_T$ . This is a consequence of the fact that with the *acceptance cuts* (Eq. (13–17)), the dominant SM background contribution arises from the  $\gamma + n$ -jets production. Since, for this process, a missing transverse momentum can arise only from mis-measurement, this contribution can be suppressed significantly by introducing a harder  $\cancel{p}_T$  cut. However, this would also reduce the signal simultaneously (see Fig. 6) and, hence, we do not impose any further missing transverse momentum cut in our analysis.

Another variable that is often used for such purposes is the effective mass. Defined as the scalar sum of the transverse momenta of all the visible particles, as well as the total missing

transverse momentum, it can be expressed, in our case, through

$$M_{\text{eff}} = \sum_j p_T^j + p_T^\gamma + \cancel{p}_T . \quad (18)$$

In Fig. 7, we show the  $M_{\text{eff}}$  distributions of the signal and background at the LHC with  $\sqrt{s} = 7$  TeV (left panel) and 14 TeV (right panel) respectively. Expectedly, the distribution is flatter for larger  $R^{-1}$  (see Fig. 7b). And, while it may seem that, for  $\sqrt{s} = 7$  TeV, the signal distribution does rise above the background, note that this is true only for a relatively low value of  $R^{-1}$ . Furthermore, with the peak position being a strong function of  $R^{-1}$ , a cut on  $M_{\text{eff}}$  would be effective only if it is designed accordingly. In other words, such a cut would not be very useful tool in search strategies.

Finally, we consider the ratio  $\cancel{p}_T/M_{\text{eff}}$ , and in Fig. 8, present the distributions in the same. The background peaks around  $\cancel{p}_T/M_{\text{eff}} \sim 0.1$  and it is obvious that it would be reduced significantly if a lower bound on this ratio is imposed this ratio. To be specific In our analysis, we require that

$$\frac{\cancel{p}_T}{M_{\text{eff}}} \geq 0.2 \quad (19)$$

Therefore, our final event *selection criteria* consists of the *acceptance cuts* (viz. Eq. (13–17)) alongwith Eq.(19). In Table 2, we summarize the signal and the SM background cross-sections, for two operative energies of the LHC, after the imposition of all of these cuts. It is very evident that more than  $5\sigma$  discovery for  $R^{-1} = 500$  GeV is possible with the integrated luminosity of  $2\text{fb}^{-1}$  at the LHC with  $\sqrt{s} = 7$  TeV. On the other hand, if the LHC reaches  $\sqrt{s} = 14$  TeV, we will be able to probe  $R^{-1}$  upto 1000 GeV with an integrated luminosity of  $20 \text{fb}^{-1}$ .

#### 4.1 Possibility of mass measurement/ parameter determination

The search strategy, presented above, does not depend on looking for any bump or edges. Consequently, a direct determination of masses or mass differences is not straightforward. Rather, the analysis is of the number counting type and, thus, depends crucially on an accurate estimation of the SM backgrounds. In particular, both signal and background comprise of multiple particle production of varied type, as well as cascade decay chains. And last but not the least, is the fact that the whole analysis pertains to a hadron collider, where any theoretical prediction of number of events/cross-section is to be accepted with

Cross-section in fb					
$\sqrt{s} = 7$ TeV			$\sqrt{s} = 14$ TeV		
Background	$R^{-1}$	Signal	Background	$R^{-1}$	Signal
in fb	GeV	[fb]	[fb]	GeV	[fb]
12.12	300	73.1	47.88	500	265.1
	500	17.5		750	43.9
				1000	9.4

Table 2: Signal and SM background cross-sections (in fb) after the *selection cuts* for different values of  $\sqrt{s}$  and  $R^{-1}$ .

the uncertainties of parton distribution, choice of scales etc. Interplay of these two effects prevents a determination of masses from the cross-section measurement itself.

However, a careful look at the  $M_{\text{eff}}$  (defined in Eq. (18)) distributions in Fig. 7, leads us to a possible correlation between the peak position ( $x_0$ ) of such distributions with respective  $R^{-1}$  values.

Naively, one would expect this correlation to become stronger once the cut of Eq.(19) is imposed, and this, indeed, turns out to be the case. However, before we attempt to establish this correlation, we turn to the question of multiple particle production channels contributing to the signal, for, despite the KK spectrum being relatively degenerate, multiple peaks would still be expected. To examine this, we consider, individually, each of the major production channels contributing to the signal. After background removal, the excess is then fitted with a Gaussian. Remarkably, the peak positions are not too different. This is illustrated in Figs. 9, wherein we present the  $M_{\text{eff}}$  distributions for two different values of  $R^{-1}$  (500 GeV and 750 GeV) wherein both the total signal (adding up all the sub-processes) and the contribution from  $G_\mu G_\mu$  production alone have been presented separately. Note that  $G_\mu G_\mu$  corresponds to the heaviest masses corresponding to a particular choice of parameters, and thus, represents the maximum deviation from the overall sum. This small difference is, of course, reflective of the relative degeneracy of the spectrum. Furthermore, the absence of any discernible thresholds (or the existence of multiple peaks) in the distribution for the entire signal, is a consequence of the twin facts that the separations between the peaks is much smaller than the widths of the individual distributions and that no dominant peak exists

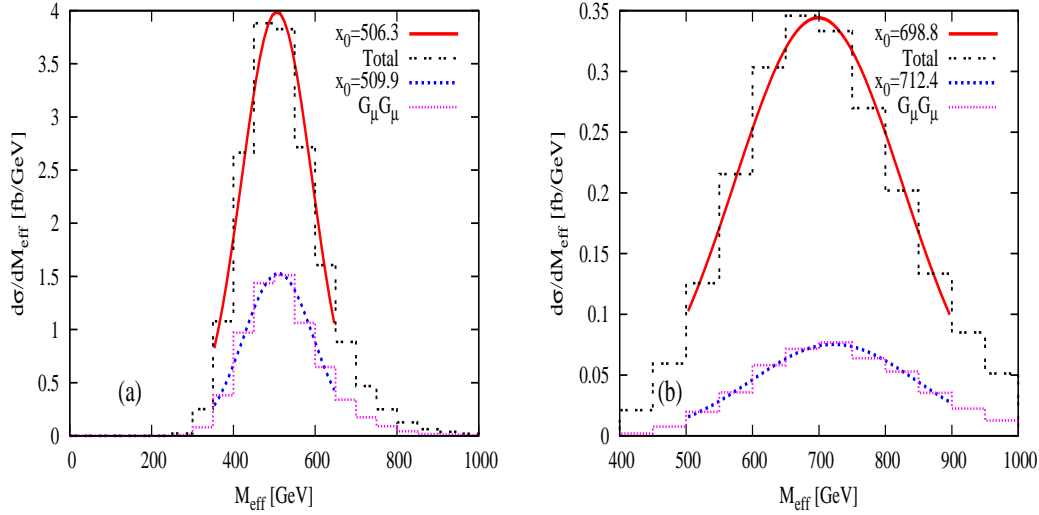


Figure 9: The total  $M_{eff}$  distributions and contribution from  $G_\mu G_\mu$  production for  $R^{-1} = 500$  GeV (left panel) and 750 GeV (right panel) with  $M_s = 10R^{-1}$  at the LHC with center-of-mass energy 14 TeV.  $x_0$  stands for the peak position of the respective fitted Gaussian distribution.

below the  $G_\mu G_\mu$  one.

A few points need to be made at this juncture. The relative importance of the  $G_\mu G_\mu$  channel might seem unwarranted in view of the fact that this does not represent the dominant production process (see Fig.3). However, note that one of the two dominant mass splittings in the theory is that between the  $G_\mu$  and  $Q_\pm$ . Consequently, the jet from the  $G_\mu \rightarrow Q_\pm$  decay is a energetic one. Thus, the requirement of four jets with  $p_T > 30$  GeV preferentially selects  $G_\mu G_\mu$  events, thereby according it far greater importance. The relatively large separation between the  $G_\mu G_\mu$  peak and the overall peak for a larger  $R^{-1}$  value (compare Figs. 9 a & b) is also a testament to this, for a larger  $R^{-1}$  implies a larger absolute split between the different level-(1,0) fields, leading to harder jets all around. However, even for  $R^{-1} = 1$  TeV, the difference is comparatively small when compared to experimental resolutions. The final point relates to the fact that peak in  $M_{eff}$  is closer to the masses of the particle produced rather than twice the mass. This is not unexpected, given the fact that the spectrum is so degenerate (and, consequently, softer jets) and that the two contributions (emanating from the two  $B_H^{(1,0)}$ ) to missing  $p_T$  cancel each other to a significant extent. Indeed, the situation is somewhat analogous to that in Ref. [33].

It ought to be remembered that, for a given  $R^{-1}$ , the quantum corrections to the masses

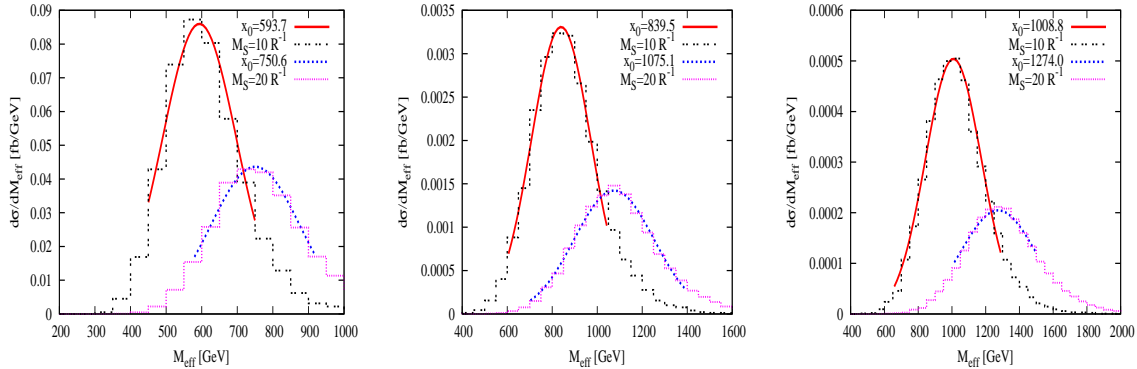


Figure 10: The  $M_{eff}$  distributions (calculated using only the  $G_\mu G_\mu$  sub-process) for different values of  $R^{-1}$  ( $= 600, 900, 1100$  GeV) and cut-off  $M_s$  ( $= 10R^{-1}$  and  $20R^{-1}$ ) at the LHC with center-of-mass energy 14 TeV.

(and, hence, the splitting between them) grows with the value of the cut-off  $M_s$ . With the loss of degeneracy, the position of the  $M_{eff}$  peak would move upwards. This is amply demonstrated by Fig.10, wherein we present the  $M_{eff}$  distribution for the signal (on imposition of all the selection cuts) alongwith the Gaussian fit. We have chosen to use only the  $G_\mu G_\mu$  production for reasons explained above.

In Fig.11, we exhibit the relation between  $R^{-1}$  and the fitted peak position (denoted  $x_0$ ). The linear dependence is understandable given the dependence of the masses on the compactification radius. As could already be expected from a study of Fig.10, the exact linear relation (i.e., the coefficients) does depend on the cutoff scale. Given this, it is obvious that an accurate extraction of  $R^{-1}$  (equivalently, the common mass scale) is not possible from this measurement alone. However, given that  $M_s R$  cannot be too large, the inaccuracy, as suggested by Fig. 11, is perhaps not too large for a first estimate. An unique determination is possible only with further experimental data. This could come about in a variety of ways. For example, an accurate measurement of the signal cross section would provide us with supplementary information about the mass scale<sup>6</sup>. Similarly, the discovery of any substructure in the  $M_{eff}$  distribution would hint at (some of) the mass differences. And, finally, the use of other final states would provide additional information. However, given that ours is only a preliminary study, we desist from a more complete examination of this

---

<sup>6</sup>While both the position of the peak and its height depend on  $R^{-1}$  as well as  $M_s R$ , the dependences are different.



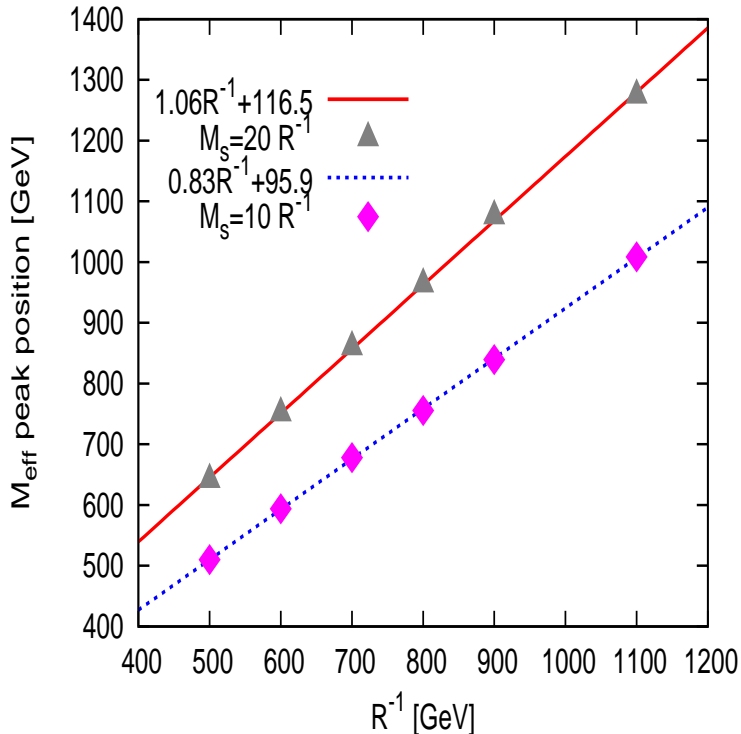


Figure 11: Correlation between the peak of  $M_{eff}$  distributions and  $R^{-1}$ .

issue, for that demands a detailed study inclusive of higher order effects on the one hand and detector simulation on the other.

## 5 Summary and Conclusion

To summarise, we have investigated the possibility of discovering the Universal Extra Dimensional Model with 2 extra space-like dimensions at the LHC. We have considered the production of strongly interacting  $(1, 0)$ -mode particles, namely the KK-excitations of gluons and quarks of first two generations. At the LHC, the total production cross-section of such strongly interacting particles is quite large. Once produced, these decay to SM gluons and quarks along with  $(1, 0)$ -mode EW gauge bosons/adjoint scalars. Further decays of these gauge bosons and scalars will produce leptons and photons. Of particular interest is the fact that the  $B_{\mu}^{(1,0)}$  (KK-excitation of the  $U(1)$  gauge boson) decays into a photon and  $B_H^{(1,0)}$ , the latter being the lightest KK-particle. In this article, we concentrated on a final state comprising of multiple jets along with a single hard photon and missing transverse energy

(due to the production of a pair of  $B_H^{(1,0)}$  as the end products of the decay chains ). There are several Standard Model backgrounds which can mimic similar final states in the detector. We have estimated cross-sections for the signal processes using CALCHEP [31] whereas the SM background processes have been estimated using ALPGEN [29] and MADGRAPH [32]. While several different processes contribute to the background, the dominant source is the SM process  $pp \rightarrow Z\gamma + n\text{-jets}$ . Comparing several kinematic distributions for signal and background processes we devise kinematic cuts to enhance the signal to background ratio. The analysis reveals that the running LHC experiment at 7 TeV (14 TeV) will explore or exclude 2 UED models with  $R^{-1}$  upto 700 GeV (1 TeV).

There are a few things which need to be mentioned here. The signal we have investigated in this article is, in a sense, complementary to that in Ref. [22], in which the production and decay of  $(1,0)$ -mode electroweak particles have been discussed. Although it is certainly true that their signal (leptons with multijets and missing transverse energy) has a better mass reach, it should be recognized that the said signal is generic to a wide variety of new physics scenarios. And while such models can, in principle, be distinguished from most of the popular supersymmetric scenarios by virtue of the relatively closely packed spectrum, the said signal would also arise in the one-dimensional UED model as well. It is here that the virtue of the hard photon in our final state (arising from the decay  $B_\mu^{(1,0)} \rightarrow B_H^{(1,0)} + \gamma$ ) lies. As such a hard photon would not arise in the minimal UED models, this affords us a possible means of distinguishing between these two scenarios.

At this stage, it would not be very irrelevant to comment on a very similar model [34], in which mUED is embedded in a higher dimensional manifold with a flat geometry. As a result,  $B_\mu^{(1)}$ , the lightest of the SM KK-excitations, is not stable any more, but decays to a photon and a graviton with a 100% branching ratio. Consequently, in such a model, two hard photons emerge in the final state, with missing energy resulting from the gravitons. While such a final state can occur in the 2UED scenario as well, (if both decay chains end in  $B_\mu^{(1,0)} \rightarrow B_H^{(1,0)} + \gamma$ ), note that this particular chain has a relatively small cumulative branching fraction. As a result, final states with a single photon (along with multijets and missing transverse energy) will far outnumber those with a pair of such photons. Such a hierarchy in the final state is quite the opposite of the situation of Ref. [34], thereby allowing to differentiate between these two scenarios as well<sup>7</sup>.

---

<sup>7</sup>The situation for gauge mediated supersymmetry breaking models is similar to that in Ref. [34], except

Finally, we have shown that there exists a correlation between the peak position of  $M_{eff}$  distribution and  $R^{-1}$ . However, the above peak position also depends on the cut-off scale  $M_s$ . Consequently, it would not be possible to determine  $R^{-1}$  or  $M_s$  only by measuring the  $M_{eff}$  distribution. An unambiguous measurement of parameters thus calls for further experimental measurement of quantities depending on these two parameters.

## 6 Acknowledgments

DC acknowledges illuminating discussions with Mihoko Nojiri, Yasuhiro Okada and Kohsuke Tobioka. AD acknowledges partial financial support from the UGC-DRS programme of the Department of Physics, Calcutta University. DKG acknowledges partial support from the Department of Science and Technology, India under the grant SR/S2/HEP-12/2006. DKG also thanks the High Energy Physics Group of ICTP for hospitality at a later stage of the project. KG was partially supported by funding available from the Department of Atomic Energy, India, for the Regional Centre for Accelerator-based Particle Physics (RECAPP), Harish-Chandra Research Institute. Authors would like to thank A. Kundu for pointing out a typo in the legend of Fig.11.

## References

- [1] N. Arkani-Hamed, S. Dimopoulos and G. R. Dvali, Phys. Lett. B **429**, 263 (1998);  
I. Antoniadis, N. Arkani-Hamed, S. Dimopoulos and G. R. Dvali, Phys. Lett. B **436**, 257 (1998)
- [2] L. Randall and R. Sundrum, Phys. Rev. Lett. **83**, 3370 (1999);
- [3] T. Appelquist, H. C. Cheng and B. A. Dobrescu, Phys. Rev. D **64**, 035002 (2001);  
H. C. Cheng, K. T. Matchev and M. Schmaltz, Phys. Rev. D **66**, 056006 (2002).
- [4] K. R. Dienes, E. Dudas and T. Gherghetta, Nucl. Phys. B **537**, 47 (1999)
- [5] K. R. Dienes, E. Dudas and T. Gherghetta, Phys. Lett. B **436**, 55 (1998);
- [6] G. Bhattacharyya, A. Datta, S. K. Majee and A. Raychaudhuri, Nucl. Phys. B **760**, 117 (2007).

---

that the spectrum is not as degenerate.

- [7] G. Servant and T. M. P. Tait, Nucl. Phys. B **650**, 391 (2003).
- [8] K. Kong and K. T. Matchev, JHEP **0601**, 038 (2006).
- [9] M. Kakizaki, S. Matsumoto and M. Senami, Phys. Rev. D **74**, 023504 (2006) [arXiv:hep-ph/0605280].
- [10] G. Belanger, M. Kakizaki and A. Pukhov, arXiv:1012.2577 [hep-ph].
- [11] G. Burdman, B. A. Dobrescu, E. Ponton, JHEP **0602**, 033 (2006).
- [12] B. A. Dobrescu, E. Ponton, JHEP **0403**, 071 (2004).
- [13] T. Appelquist, B. A. Dobrescu, E. Ponton and H. U. Yee, Phys. Rev. Lett. **87**, 181802 (2001).
- [14] B. A. Dobrescu and E. Poppitz, Phys. Rev. Lett. **87**, 031801 (2001).
- [15] B. A. Dobrescu, D. Hooper, K. Kong and R. Mahbubani, JCAP **0710**, 012 (2007).
- [16] G. Burdman, B. A. Dobrescu and E. Ponton, Phys. Rev. D **74**, 075008 (2006) [arXiv:hep-ph/0601186].
- [17] B. A. Dobrescu, K. Kong and R. Mahbubani, JHEP **0707**, 006 (2007) [arXiv:hep-ph/0703231].
- [18] A. Freitas and K. Kong, JHEP **0802**, 068 (2008) [arXiv:0711.4124 [hep-ph]].
- [19] H. Dohi and K. y. Oda, Phys. Lett. B **692**, 114 (2010) [arXiv:1004.3722 [hep-ph]].
- [20] K. Ghosh and A. Datta, Nucl. Phys. B **800**, 109 (2008) [arXiv:0801.0943 [hep-ph]].
- [21] K. Ghosh and A. Datta, Phys. Lett. B **665**, 369 (2008) [arXiv:0802.2162 [hep-ph]].
- [22] K. Ghosh, JHEP **0904**, 049 (2009)
- [23] E. Ponton and L. Wang, JHEP **0611**, 018 (2006) [arXiv:hep-ph/0512304].
- [24] D. N. Spergel *et al.* [ WMAP Collaboration ], Astrophys. J. Suppl. **170**, 377 (2007).
- [25] J. Pumplin, D. R. Stump, J. Huston, H. L. Lai, P. M. Nadolsky and W. K. Tung, JHEP **0207**, 012 (2002).
- [26] D. Stump, J. Huston, J. Pumplin, W. K. Tung, H. L. Lai, S. Kuhlmann and J. F. Owens, JHEP **0310**, 046 (2003).
- [27] H. Murayama, M. Nojiri, K. Tobioka, [arXiv:1107.3369 [hep-ph]].
- [28] B. Bhattacharjee and K. Ghosh, Phys. Rev. D **83**, 034003 (2011).

- [29] M. L. Mangano, M. Moretti, F. Piccinini, R. Pittau and A. D. Polosa, *JHEP* **0307**, 001 (2003).
- [30] CMS Collaboration, *Electron reconstruction and identification at  $\sqrt{s} = 7$  TeV*, Report No. CMS PAS EGM-10-004 (2010).
- [31] A. Pukhov, arXiv:hep-ph/0412191.
- [32] T. Stelzer and W. F. Long, *Comput. Phys. Commun.* **81**, 371 (1994).
- [33] K. Ghosh, S. Mukhopadhyay, B. Mukhopadhyaya, *JHEP* **1010**, 096 (2010).
- [34] C. Macesanu, C. D. McMullen and S. Nandi, *Phys. Lett. B* **546**, 253 (2002); C. Macesanu, A. Mitov and S. Nandi, *Phys. Rev. D* **68**, 084008 (2003).